

Dynamic Robot Motion Prediction Updates in Physical Human-Robot Interactive Tasks

Shuangda Duan, Longxin Chen, Yaqian Wang, Xuan Zhao, and Juan Rojas.

Abstract—Human-robot collaboration is on the rise. Robots need to increasingly improve the efficiency and smoothness with which they assist humans by properly anticipating a humans intention. To do so, prediction models need to increase their accuracy and responsiveness. This work builds on top Interaction Movement Primitives with phase estimation and re-formulates the framework to use dynamic human-motion observations. Previously, the probabilistic framework has only considered static human observations. By using dynamic observation windows, a series of updated human motion distributions are generated. Phase estimates occur within the dynamic time window range. Co-activation is performed between the current robot motion distribution and the newest and most probable distribution for the latest dynamic observation. The results is a smooth update of the robot motion generation that achieves high accuracies and enhanced responsiveness.

I. INTRODUCTION

In human-robot interaction (HRI) and human-robot collaboration (HRC) anticipation is desirable as it promotes the robot’s responsiveness leading to smoother collaboration. Anticipation is the result of predictions that a robot has to make as it observes its human counter-part. One of the main drawbacks of prediction however is the trade-off between achieved goal-pose accuracy and longer observation periods. The sooner a human trajectory is predicted, the quicker a robot can offer assistance. However, quick predictions can lead to robot motions that lack accuracy; whilst longer observations achieve higher accuracy at the expense of lags in responsiveness. Most of the work in HRI anticipation use fixed-time human observation windows. In this work we introduce dynamic-time human observation windows as the general-case scenario for agent observations (static windows are just a special case).

In HRI and HRC, numerous approaches have been used to generate robot motion in response to human motion observations. The research is characterized by estimating the human state to generate an appropriate and corresponding robot motion. Works like Interaction Probabilistic Motion Primitives (IProMPs) [1]–[3] generate predictive robot motions based on fixed observations of human motions to achieve physical interaction such as handover tasks. Interactive meshes (IMs) [4] learn an interaction model from human-to-human demonstrations that can be used to continuously update a robot’s motion during collaborative tasks. IMs model complex interactions however they seem to lack (timely) responsiveness. This work focuses on anticipating human motions and achieving more temporally-and-spatially responsive single-motion interactions. Other predictive works have focused on optimizing safety and avoiding predicted

human-occupancy spaces to avoid collisions [5]–[7]. This work is also not concerned with human-robot prediction at the task planning level [8] but rather generating reactive predictions within single motions. In [9], Parascho’s *et al.* introduced the Probabilistic Movement Primitives (ProMPs) framework to compose complex robot skills from basic movements in a modular control architecture. The framework provided a single unified formulation that enabled probabilistic operations to support parallel co-activation of MPs in a smooth way. Tasks could then be generated as sequences of simple or simultaneously activated skills. Adaptations to new tasks or speed are also possible by conditioning on the desired target’s positions or velocities. IProMPs were initially presented in [1]. The goal of the framework is to enable a robot assistant to adapt and learn new interactive skills on demand. Imitation learning is leveraged in collaboration tasks and ProMPs are used to generate distributions from human motion observations. The distributions serve as a prior model in a lower dimensional weight space. The model is used to recognize the intended motion of the human agent and to generate a movement primitive for the robot. By using the IProMP framework, trajectories from the human and the robot can be naturally correlated thus simplifying the framework’s complexity. Maeda *et al.* extended the IProMP framework to track human movement progress [2]. A temporal rescaling factor is estimated through human observations to improve the robot motion regression. The observation however is static. Only a single human-motion observation is used to regress the corresponding robot motion. The system is unable to dynamically adapt its prediction given new observations. More recently in [10], Manschitz *et al.* adapt DMP motions to adapt to different objects by learning to continuously activate a set of attractors over time by solving a convex optimization problem. The attractors can be represented in different coordinate frames and co-articulated movements are supported explicitly. The work assumes complete distributions from time-aligned demonstrations as well as temporally-modulated movements. We follow a similar principle and embed it in the interactive probabilistic framework. In our work, we generate new sets of possible robot distributions from updated dynamic human motion observations and use the blending concepts introduced in [9] to combine a current distribution and the distribution with the highest confidence to produce smooth updates.

In this work we study if a dynamic time-window of human observations can yield high accuracies—as those with

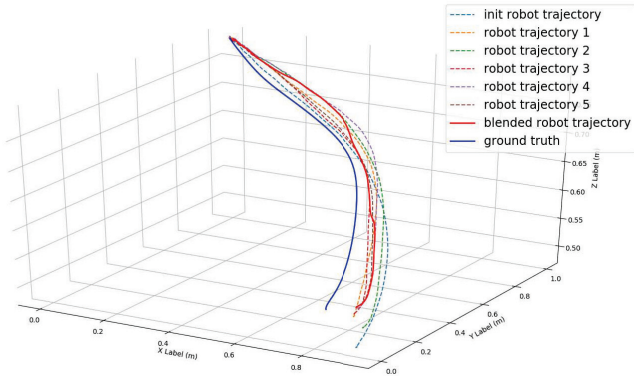


Fig. 1. A 5-time co-activated motion primitive. Over the course of the handover task, a total of five observations were obtained dynamically. With each observation a new trajectory was regressed. Co-activation occurs according to Eqn. 19

full observations—while maintaining temporal responsiveness and good phase estimation in the robot’s motion. Our contribution extends the Interactive Primitives formulation via Probabilistic Movement Primitives to use a dynamic time-window for human observations whereby new distributions are generated with each new observation and robot motions are co-activated smoothly to the most confident target distribution. We also contribute a metric that aids in the selection of a time-window duration that minimizes positioning and phase estimation errors.

We use the IProMP framework with phase estimation to model MPs via Gaussian distributions. Human observations are captured through a dynamic time-window whose duration is determined by a parameter (Sec. II-B). Phase estimation is limited to the dynamic window duration (Sec. II-C). Once the human observation is updated based on the human phase, we perform the robot task recognition by selecting the posterior distribution with the highest probability (Sec. II-D). Blending is then performed iteratively for each new dynamic observation (Sec. III). To blend, we co-activate the current distribution with the incoming distribution by computing the product of the distributions as a function of a smooth activation function. Fig. 1 shows how five co-activations occur in a task. The output leads to a smooth transition towards the newly updated robot trajectory. In our experiments (Sec. IV) we compare the performance of the dynamic time-window IProMP formulation with that of a static time-window formulation across two experiments: (a) tasks with a uniform trajectory pattern and (b) tasks where trajectories are similar at the beginning of the task but diverge later in the task. For each experiment, we compare accuracy gain as a function of dynamic window-time duration for three measurements: (i) robot joint angle configuration at each time-step, (ii) Cartesian position at the final goal position, and (iii) phase estimation error. Finally, a weighted sum error metric is used to select the most optimal dynamic window time duration across all metrics. We found that on average for the dynamic time window formulation, we reach accuracy positioning levels that are only possible for the

static window case when 90% or more of the observations are available for the human motion. We also found that the dynamic formulation yields a much more responsive system; one that is able to adapt correctly in situations where multiple learned human distributions initiate with similar paths but deviate later in the trajectory. Our work thus shows that more accurate and responsive motions can be attained in probabilistic formulations for HRI/HRC by dynamically updating the human observations.

Our paper is organized as follows: in Sec. II, we introduce the Probabilistic Motion Primitives framework and its extensions to Interaction Primitives and Phase Estimation. In Sec. III, we explain how blending can be done for dynamic observation settings. Sec. IV presents two experiments and associated results. Finally, in Sec. V we highlight key lessons learned in this work.

II. INTERACTION MOTION PRIMITIVES WITH PHASE ESTIMATION AND DYNAMIC OBSERVATIONS

In HRC tasks, IProMPs generate a robot collaborative motion based on the prediction from a set of partial human motion observations. In this section, we introduce IProMPs by first explaining probabilistic motion primitives for single dimensions, then describe the formulation for interactive scenarios, then incorporate phase estimation with dynamic time-window human observations, and conclude with parameter learning.

A. Probabilistic Movement Primitives for a Single Dimension

ProMPs summarize patterns across demonstrations in a probabilistic manner. ProMPs capture correlations across data dimensions leading to a probability distribution over trajectories. Representing variance information correctly is critical as it reflects variations in movement execution across time steps. For each time step, a single dimension position is represented by $y_t \in \mathbb{R}^1$ and a trajectory of T time steps as $\mathbf{y}_{1:T}$. A parameterization of $\mathbf{y}_{1:T}$ in a lower dimensional weight space is given as a linear basis function model of n Gaussian basis functions and weights $\boldsymbol{\omega}$ according to:

$$y_t = \boldsymbol{\psi}_t^T \boldsymbol{\omega} + \epsilon_y, \quad (1)$$

$$p(\mathbf{y}_{1:T} | \boldsymbol{\omega}) = \prod_1^T \mathcal{N}(y_t | \boldsymbol{\psi}_t^T \boldsymbol{\omega}, \sigma_y),$$

where, $\epsilon_y \sim \mathcal{N}(0, \sigma_y)$ models zero-mean i.i.d. Gaussian noise. The set $\boldsymbol{\psi} = [(\psi_t)_1, (\psi_t)_2, \dots, (\psi_t)_N]^T \in \mathbb{R}^{N \times 1}$ contains values of each of the basis function at time t . Given a basis function, one can compute $\boldsymbol{\omega}$ for each trajectory $\mathbf{y}_{1:T}$ using linear regression with a time-dependent design matrix:

$$\boldsymbol{\omega} = (\boldsymbol{\Psi}_{1:T}^T \boldsymbol{\Psi}_{1:T})^{-1} \boldsymbol{\Psi}_{1:T} \mathbf{y}_{1:T}, \quad (2)$$

where,

$$\boldsymbol{\Psi}_{1:T} = \begin{bmatrix} (\psi_1)_1 & \cdots & (\psi_1)_N \\ \vdots & \ddots & \vdots \\ (\psi_T)_1 & \cdots & (\psi_T)_N \end{bmatrix} \quad (3)$$

The ω vector can compactly represent a single trajectory as the number of basis functions is often much lower than the number of trajectory steps*. Having a set of motion trajectories, we can compute a probability distribution over the weights ω . To capture the variance across trajectories in different demonstrations, we define θ as a parameter that governs the distribution of weight vectors in the set ω and we assume that $\omega \sim \mathcal{N}(\mu_\omega, \Sigma_\omega)$, that is $\theta = (\mu_\omega, \Sigma_\omega)$.

The trajectory distribution $p(\mathbf{y}_{1:T}; \theta)$ can now be computed by marginalizing out the weight vector ω . The distribution $p(\mathbf{y}_{1:T}; \theta)$ defines a Hierarchical Bayesian Model (HBM) whose parameters are given by the observation noise variance σ_y and the parameters θ of $p(\omega; \theta)$. We compute the probability distribution of a position at a given time from the ω distribution as

$$p(y_t|\theta) = \int p(y_t|\omega)p(\omega|\theta)d\omega \quad (4)$$

$$= \mathcal{N}(y_t|\psi_t^T \mu_\omega, \psi_t^T \Sigma_\omega \psi_t + \sigma_y).$$

The above distribution captures spatial correlations across a set of demonstrations. To cope with demonstrations of varying durations the training set is time aligned.

B. Human and Robot Movement Correlations in an Interaction Model

We now extend ProMPs to a multidimensional setting and compute the correlation for the full set of data-dimensions for human and robot motions across demonstrations. Note the work assumes that human-motion collaborative-task trajectories differ spatio-temporally from one another. Under this assumption, the use of motion information is sufficient to distinguish distinct tasks. However, if the assumption is violated and different tasks share similar trajectories, the task recognition system will fail. Our work in [11] addressed this limitation.

IProMPs model the correlation across multiple dimensions. Each dimension is given by each of agent's degrees-of-freedom (DoFs). We define the state vector \mathbf{y}_t as a concatenation of the observed P number of human DoFs, followed by the Q DoFs of the robot:

$$\mathbf{y}_t = [y_{1,t}^H, \dots, y_{p,t}^H, y_{1,t}^R, \dots, y_{q,t}^R]^T, \quad (5)$$

where, $(\cdot)^H$ refers to the human position and $(\cdot)^R$ refers to the robot joint angle configuration. The weight vector ω is the concatenation of all weight vectors involved in a given demonstration. Thus, all the interacting dimensions in a task are correlated as:

$$\omega_i^T = [(\omega_1^H)^T, \dots, (\omega_p^H)^T, (\omega_1^R)^T, \dots, (\omega_q^R)^T]. \quad (6)$$

As in the single dimension case, the weight vector is given as a linear regression model:

$$p(\mathbf{y}_t|\omega) = \mathcal{N}(\mathbf{y}_t|\mathbf{H}_t^T \omega, \Sigma_y). \quad (7)$$

*Handover tasks have an average duration of 4 seconds sampled at 50Hz leading to 200 samples. Instead we use 31 basis functions, thus only using 16% of the original sample size

\mathbf{H}_t is the time-dependent basis matrix for the human and robot observations and defined as:

$$\mathbf{H}_t = \text{diag}((\psi_t^T)_1, \dots, (\psi_t^T)_p, (\psi_t^T)_1, \dots, (\psi_t^T)_q). \quad (8)$$

Given partial human observations, the posterior distribution is computed using a Kalman Filter (robot observations are set to zero) yielding:

$$\mathbf{y}_t^o = [\mathbf{y}_{1,t}^H, \dots, \mathbf{y}_{p,t}^H, \mathbf{y}_{1,t}^R, \dots, \mathbf{y}_{q,t}^R]^T. \quad (9)$$

To contrast with a complete observation sequence $[t : t']$, the notation $[t - t'] \in \mathbb{R}^{s \times (p+q)}$ is used to indicate a sequence s of partial observations in the interval. Observations can be considered as modulations to via-points. The operation is done by conditioning the ProMPs to reach a certain state $\mathbf{y}_{t-t'}^o$ at time $(t - t')$. The conditioning adds a desired observation to $\mathbf{x}_{t-t'} = [\mathbf{y}_{t-t'}^o, \Sigma_y^o]$ to the probabilistic model and applies Bayes theorem. Kalman filtering is used to compute the posterior distribution according to:

$$\begin{aligned} \mu_\omega^{new} &= \mu_\omega + \mathbf{K}(\mathbf{y}_{t-t'}^o - \mathbf{H}_{t-t'} \mu_\omega), \\ \Sigma_\omega^{new} &= \Sigma_\omega - \mathbf{K}(\mathbf{H}_{t-t'} \Sigma_\omega). \end{aligned} \quad (10)$$

Here, $\mathbf{K} = \Sigma_\omega \mathbf{H}_{t-t'}^T (\Sigma_y^o + \mathbf{H}_{t-t'} \Sigma_\omega \mathbf{H}_{t-t'}^T)^{-1}$. Since missing robot observations exist, for each time step of the observation matrix we set $\mathbf{H}_{t-t'}$ as:

$$\mathbf{H}_{t-t'} = \begin{bmatrix} (\psi_t^T)_1 & \dots & 0 & 0 & \dots & 0 \\ 0 & \ddots & 0 & 0 & \ddots & 0 \\ 0 & \dots & (\psi_t^T)_p & 0 & \dots & 0 \\ 0 & \dots & 0 & 0_1 & \dots & 0 \\ 0 & \ddots & \vdots & 0 & \ddots & 0 \\ 0 & \dots & 0 & 0 & \dots & 0_q \end{bmatrix} \quad (11)$$

with $\mathbf{H}_{t-t'} \in \mathbb{R}^{(p+q) \times (p+q)N}$.

C. Phase estimation with Dynamic Observation Windows

Humans normally execute repetitions of specific tasks at different speeds. This facts leads to uncertainty in the demonstration's time duration. To capture the task's spatial variation correctly, time alignment must be done. Additionally, the phase of human observations (at test time) must be estimated to align it to that of trained spatial models.

In Maeda's *et al.* original work [2], each demonstration using static observation windows (SOW) was resampled yielding a nominal duration T_{nom_sow} . We adjust the definition of the nominal duration to fit the length of the dynamic observation window (DOW) duration yielding T_{nom_dow} . For each i^{th} demonstration, we assume constant temporal changes in relation to the nominal duration. Eqtn. 12 thus introduces a temporal scaling factor to index demonstrations according to the nominal DOW time index.

$$\alpha_{i_dow} = T_i / T_{nom_dow}. \quad (12)$$

To determine the best phase estimate during test time, we use the single phase temporal model in [2]. A distribution of phase ratios across demonstrations is modeled as

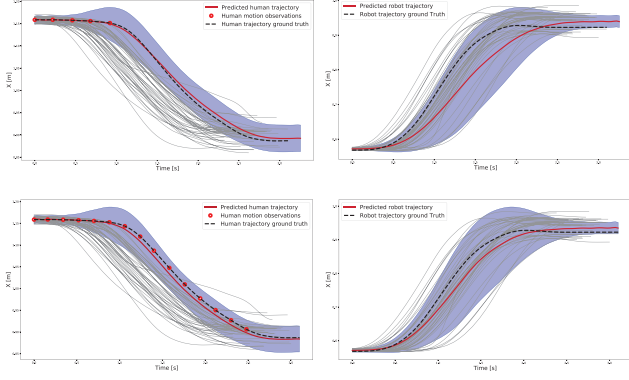


Fig. 2. Examples of two different phase estimates for the handover task with the same test data. The upper row depicts handovers with five human observations up to 1 second of the human motion (used $down_t = 0.2$). The bottom row contains fifteen observations up to 2.5 second of the human motion $down_t = 0.6$. Human phase estimation is on the left, while robot phase estimation is on the right. Note that with more human observations, alpha estimates yield higher accuracy. The upper row shows a 0.30s error, while the bottom row shows a 0.02s error.

a normal distribution and set as the phase prior: $\alpha_{down} \sim \mathcal{N}(\mu_{\alpha_{down}}, \sigma_{\alpha_{down}})$. Given a human observation $\mathbf{y}_{t-t'}^o$, the phase posterior is:

$$p(\alpha_{down} | \mathbf{y}_{t-t'}^o, \boldsymbol{\theta}) \propto p(\mathbf{y}_{t-t'} | \alpha_{down}, \boldsymbol{\theta}) p(\alpha_{down}), \quad (13)$$

with $p(\alpha_{down})$ as the prior for scaling factor α_{down} , and with a task-specific likelihood given by:

$$p(\mathbf{y}_{t-t'} | \alpha_{down}, \boldsymbol{\theta}) = \int p(\mathbf{y}_{t-t'}^o | \boldsymbol{\omega}, \alpha_{down}) p(\boldsymbol{\omega}) d\boldsymbol{\omega}. \quad (14)$$

So finally, the best task-specific phase estimate given the human observations on $\mathbf{y}_{t-t'}^o$ is:

$$\alpha_{down}^* = \arg \max_{\alpha_{down}} p(\alpha_{down} | \mathbf{y}_{t-t'}^o, \boldsymbol{\theta}). \quad (15)$$

Fig. 2 provides an illustration of phase estimation performance. There are two examples with the top example

D. Task Recognition

Once the best phase estimate for human observations is obtained, we must recognize the most likely task model in a set of k tasks. Task recognition also follows a probabilistic approach; we compute the posterior distribution of a task given human observations according to:

$$p(k | \mathbf{y}_{t-t'}^o) \propto p(\mathbf{y}_{t-t'}^o | \boldsymbol{\theta}_k, \alpha_{down}^*) p(k), \quad (16)$$

where, $p(k)$ is the task's prior probability and can be determined by the specific circumstances of an experiment. The likelihood of each component given the model $\boldsymbol{\theta}$ is:

$$p(\mathbf{y}_{t-t'}^o | \boldsymbol{\theta}_k, \alpha_{down}^*) = \int p(\mathbf{y}_{t-t'}^o | \mathbf{H}_{t-t'}^o \boldsymbol{\omega}, \boldsymbol{\Sigma}_y) p(\boldsymbol{\omega}; \boldsymbol{\theta}_k) d\boldsymbol{\omega}. \quad (17)$$

A task is selected by choosing the posterior with the highest probability:

$$k^* = \arg \max_k p(k | \mathbf{y}_{t-t'}^o) \quad (18)$$

Fig. II-D, illustrates a collaborative scenario for three hand-over tasks as well as human motion and the corresponding human-guided robot motion.

III. BLENDING OF MOVEMENT PRIMITIVES

In this section, we study how to continuously combine and blend different MPs into a single compounded primitive. Suppose that we have a set of i different primitives that we wish to blend. Here, when a human observation is updated, a new robot primitive is generated. Pairs of primitives can be co-activated by computing the product of their distributions. For example, $p_{new} \propto \prod_i p_i(\tau)^{a^{[i]}}$ where $a^{[i]} \in [0, 1]$ denotes the activation of the i^{th} primitive. The product captures overlapping regions of active MPs.

It's also necessary to modulate the activations of primitives. Such modulation allows to continuously blend the movement execution from one primitive to the next. To this end, a trajectory is decomposed into single time steps and uses time-varying activation functions $a_t^{[i]}$ such that product of distributions is defined as:

$$p^*(\tau) \propto \prod_t \prod_i p_i(\mathbf{y}_t)^{a_t^{[i]}}, \quad (19)$$

$$p_i((y_t)) = \int p_i((y_t | \boldsymbol{\omega}^{[i]})) p_i(\boldsymbol{\omega}^{[i]}) d\boldsymbol{\omega}^{[i]}$$

For Gaussian distributions $p_i((\mathbf{y}_t)) = \mathcal{N}(\mathbf{y}_t | \boldsymbol{\mu}_t^{[i]}, \boldsymbol{\Sigma}_t^{[i]})$, the resulting distribution $p^*(\mathbf{y}_t)$ is defined as in [9] and is again Gaussian with variance and mean:

$$\boldsymbol{\Sigma}_t^* = \left(\sum_i \left(\boldsymbol{\Sigma}_t^{[i]} / a_t^{[i]} \right)^{-1} \right)^{-1}, \text{ and} \quad (20)$$

$$\boldsymbol{\mu}_t^* = (\boldsymbol{\Sigma}_t^*) \left(\sum_i \left(\boldsymbol{\Sigma}_t^{[i]} / a_t^{[i]} \right)^{-1} \boldsymbol{\mu}_t^{[i]} \right).$$

As for the activation function used in this work we use a pair of sigmoid functions to define a rising edge and a falling edge:

$$S(t) = \frac{1}{1 + e^{-lt}} \text{ and} \quad (21)$$

$$S(t) = \frac{1}{1 + e^{lt}}.$$

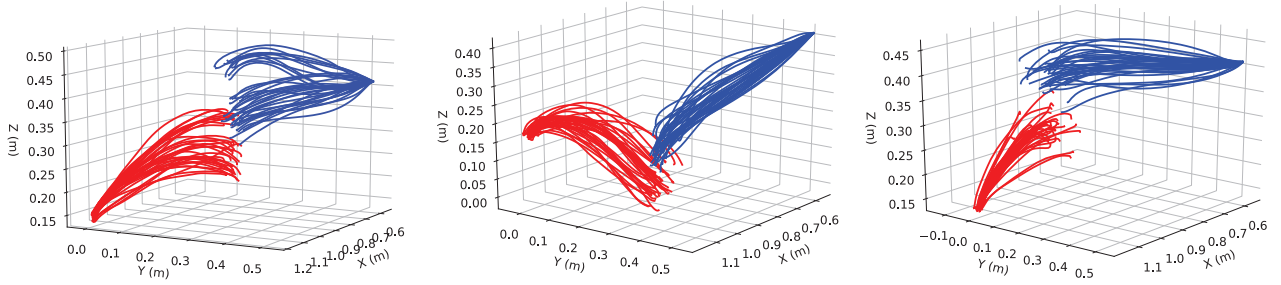
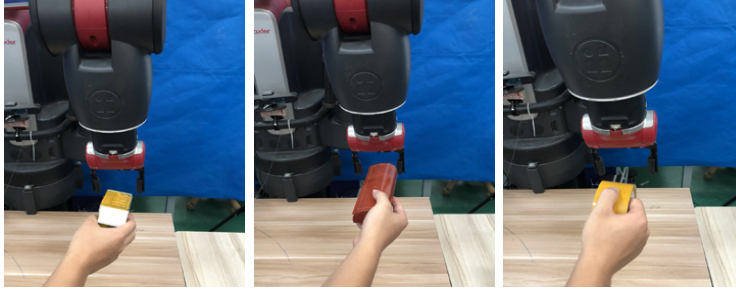
where, l denotes the gradient of the activation function.

A. Error Metric

In this work we formulate a metric to measure which dynamic observation time-window duration will perform best for in our predictive formulation. Before introducing the metric, we present the performance measurements used in this work and some explanations for how they are measured in the dynamic case and the static case which serves as a baseline.

To measure the performance of the dynamic time-window formulation we make use of three measurements:

- 1) e_p Cartesian position final goal accuracy.
- 2) e_q Joint angle configuration error sum at each time-step.



3) e_ϕ Phase estimation error at the goal position.

For each of these three measurements we compute the difference between a corresponding ground-truth and the actual goal position.

Furthermore, we are interested in computing the performance gains of the dynamic formulation over that of the static one. For each of the three aforementioned measures we compute the difference between the static and the dynamic results *i.e.*

$$\begin{aligned} \nabla e_p &= e_{p_{sow}(f)} - e_{p_{dow}_t} \\ \nabla e_q &= e_{q_{sow}(f)} - e_{q_{dow}_t} \\ \nabla e_\phi &= e_{\phi_{sow}(f)} - e_{\phi_{dow}_t}. \end{aligned} \quad (22)$$

Note that for the static formulation performance is reported according to the observation window percentage (observing an entire task is equivalent to observing 100% of the task) $sow(f)$. For the dynamic formulation performance is reported according to the duration of the dynamic time window dow_t . Thus to measure the performance gain in the dynamic formulation, we compute the difference in performance for the three measures using observation window percentages (static case) and different curves for dynamic window durations. Fig. 3 from the Experiments section illustrates these measurements.

In order to determine which dynamic observation time-window duration has the best performance over the three measures, we use a weighted sum of errors to define the total error measurement for a given dynamic window. The weighted error sum result for each dow_t is placed in the rows of column matrix m as shown in Eqn. 23. Then, the index with the smallest error sum is selected as the best time duration window for a given motion type.

$$\min m_{dow_t} = \gamma_p \frac{e_{p_{dow}_t}}{\max_t e_{p_{dow}_t}} + \gamma_q \frac{e_{q_{dow}_t}}{\max_t e_{q_{dow}_t}} + \gamma_\phi \frac{e_{\phi_{dow}_t}}{\max_t e_{\phi_{dow}_t}} \quad (23)$$

where, the weighting scale for each of the three measures is given by γ_i , where $i = p, q, \phi$. Each factor represents the fraction of error measure for a given dow_t with respect to the maximum error value across all dynamic window durations.

IV. EXPERIMENTS AND RESULTS

Our experimental testbed used the dual-armed humanoid Baxter robot with standard Rethink Robotics electric grippers. An ASUS Xtion Pro camera was used along with OpenNI tracker in ROS Indigo and Linux Ubuntu 14.04. As for dynamic observation window durations dow_t , this work tested a range of four discrete values in seconds: $dow_t = [1, 0.5, 0.2, 0.1]$ secs. The temporal scaling factor α_{dow} from Eqn. 12 is computed by using a nominal duration T_{nom_dow} set to the duration of the dynamic observation window. Given a dynamic time window duration dow_t , the total number of dynamic observations in a task is then the ratio of task duration to dynamic time window duration: T/dow_t . An equivalent number of co-activations are needed to update the robot's motion through the task. Finally, for the dynamic observations, beyond the duration of the window, the number of observations in a given window must be selected. For these experiments, we observed every 1-out-of-5 human joint angle readings.

Two distinct experiments are used to test the system performance. The first experiment uses simple trajectories, while the second experiment uses sets of trajectories that share similar starts but have different endings. For each demonstration, a total of 20 trials are executed. Leave-one-out cross-validation (loocv) is used for training and testing. Performance is evaluated under two modalities. First, is a direct evaluation for the dynamic formulation according to the three measures introduced in Sec. III-A. Second, is a comparative evaluation between the dynamic formulation and

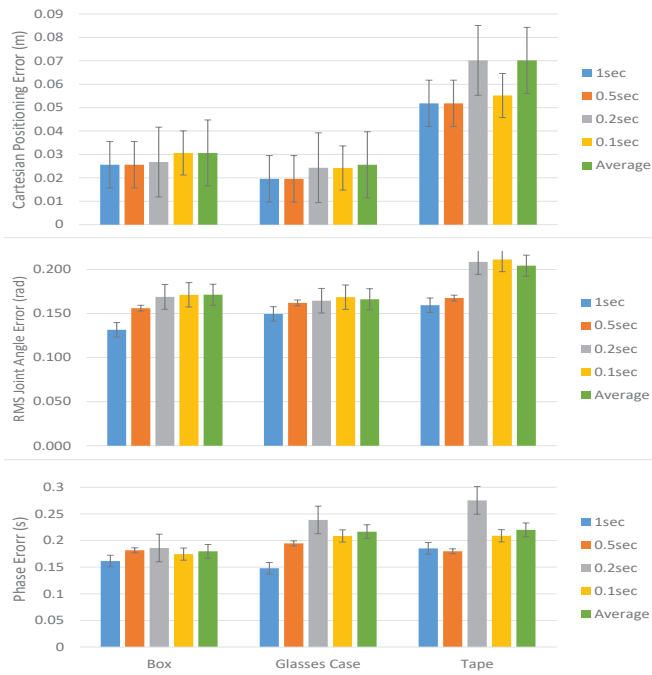


Fig. 3. Cartesian position goal errors, RMS joint trajectory errors, and phase estimation errors are shown for dynamic observation windows of four durations along with the average performance. Data is also shown for the three handover tasks explained in Sec.IV.

the static one using the same three measures.

A. Experiment 1

Exp. 1 is designed to test the accuracy of the dynamic predictions. Three collaborative handover tasks consisting of a simple box, a glasses case, and a circular masking tape are conducted as shown in Fig. II-D. For each task, the path of the trained human trajectories is unimodal; in other words, all task trials beginning and end paths are the same distribution (in Exp. 2, the ending portion of the trial trajectories diverge in different directions as seen in Fig. 5).

Results

1) *Direct Evaluation:* As summarized in Fig. 3, the dynamic formulation achieved average (of dynamic window durations) Cartesian position goal errors of (0.028, 0.023, 0.059)m; average RMS joint errors of (0.163, 0.163, 0.195)rad, and average phase estimation errors of (0.176, 0.203, 0.213)s for the box, glasses, case, and tap handovers respectively.

All the best results came from duration 1.0s (except for the phase error which came from the tape task) but notice that the difference between other window durations is not significant. This give us the flexibility to select shorter durations that increase responsiveness at the expense of a small loss in accuracy.

2) *Comparative Evaluation:* Performance comparisons for the dynamic formulation of the handover box between the static and dynamic formulations are summarized in Fig. 4. The figure has three plots for each of the three error

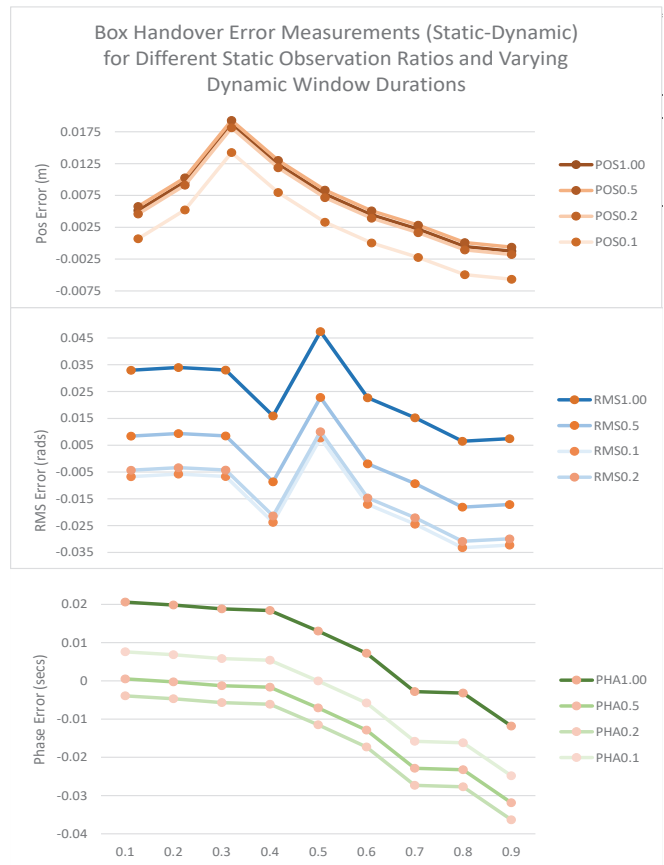


Fig. 4. Three error measurement differences between static and dynamic observation window formulations across static observation ratios (0.1 to 0.9): (top) Cartesian goal position error difference (m), (middle) RMS joint angle error difference over time steps, and (bottom) phase estimation error difference.

measure comparisons. With each plot, four curves represent four distinct dynamic observation window durations. The curves represent the difference between the static and dynamic formulations from Eqtn. 22. A positive error in the graph implies that the dynamic formulation performance outperforms the static one. The top plot, which is related to the Cartesian goal position error difference at the end of the task, shows three of the four curves are almost superimposed. This indicates that the accuracy performance of the dynamic system for durations of 1, 0.5, and 0.2 seconds was similar (ultimately each of these windows will have observed all data). For these three curves it is not until the static system observes around 80% of the trajectory that it can match the performance of the dynamic system. Given that the dynamic system can continuously update its distributions it gives the ability to increasingly approach the ground-truth while improving responsiveness.

With reference to the middle plot, we consider the RMS joint angle configuration error difference along trajectory time steps. Notice that the performance of different dynamic window durations varies in non-trivial ways. The best performance comes from the longest duration window *RMS1.00*. For this particular curve, the static formulation does not

match the performance of the dynamic window as the error difference does not reach zero by the end of the task. The reasoning is the same as that mentioned for the Cartesian goal position measure.

With respect to the bottom plot, we consider the Phase estimation error difference at the end of the task. Recall that our scaling factor α_{dow} is set by the duration of the dynamic observation window. The best performance comes from the window $PHA1.00$. This indicates that longer durations for nominal window durations assist in having better phase estimation errors. The dynamic performance was only matched by the static formulation when it observed slightly less than 70% of the trajectory.

Given these three independent error measure comparisons, we must determine which dynamic observation window performed best across all measures. Using the metric definition in Eqtn 23, we tested two γ weight combinations $\{\{0.33,0.33,0.33\}, \{0.50,0.25,0.25\}^*\}$ for our performance metric m . In all cases, dynamic observation window with 1.0 second duration had the best performance. The results from the box handover case were consistent with the results for the glasses case demonstrations and the tape demonstrations. The dynamic formulation reported similar gains across all measures.

B. Experiment 2

In Exp. 2 we test the performance of the system, through the use of four handover tasks that share similar initial trajectories but in the end diverge to leftwards, rightwards, upwards, and downwards as depicted in Fig. 5. As in Experiment 1, we perform direct evaluations and comparative evaluations. We also compare the performance of dynamic formulation in Exp. 2 with that in Exp. 1.

Results

*And all combinations of this set.

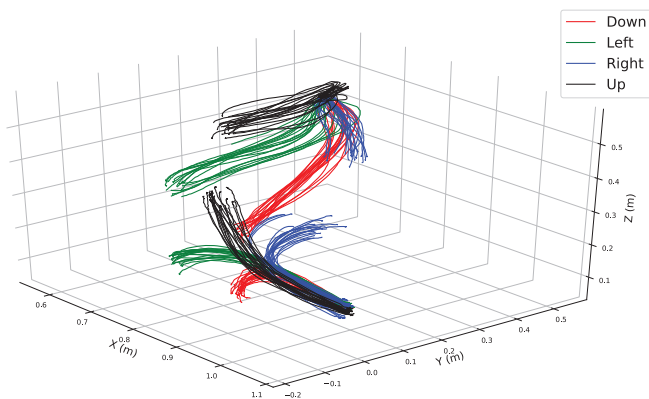


Fig. 5. Collaborative trajectories with similar human initial paths and diverging paths. The red color indicates one collaborative task, the green another one. By using static observations in the first half of the trajectory the predictive system have no better results than chance to predict the correct final position. The static system would also lack responsiveness to the changes effected by the human collaborator later in the task.

1) *Direct Evaluation*:: Table I, summarizes performance evaluation in Exp. 2 for the four tasks for the best performing dynamic observation window duration (again in all cases the 1.0s duration: If we compare the average performance

TABLE I
PERFORMANCE EVALUATION FOR OPTIMAL WINDOW DURATION IN BI-MODAL TRAJECTORIES WHICH DIVERGE RIGHT, LEFT, UP, AND DOWN. ERROR MEASURES FOLLOW DEFINITIONS PRESENTED IN SEC. III-A.

	POS	RMS	Phase
Right	0.0309	0.3467	0.1712
Left	0.0248	0.1697	0.1924
Up	0.0299	0.0686	0.2301
Down	0.0459	0.2654	0.1273
Total	0.0329	0.2126	0.1803

of Exp. 1 for the three handover tasks, with the four, more complex trajectories of Exp. 2, we learn that Exp. 2 had very similar performance: which is re-assuring as the system performs consistently across trajectories with different path patterns. In terms of final Cartesian position, Exp. 2 had an improved accuracy of 0.007m; in terms of RMS joint trajectory error at each time step, Exp. 2 had slightly lower performance with 0.032rad, and very similar phase performance with a -0.024s difference.

2) *Comparative Evaluation*:: The comparative evaluation between the dynamic and static formulations is more complicated given that we have 3 tasks in Exp. 1 and 4 in Exp. 2 and we are considering the 4 window durations and the observation ratios for the static case. As with our direct evaluation, we resort to presenting average results and commenting in interesting cases. As in Exp. 1, Fig. 6, presents the comparative performance between average static results and average dynamic results. These results are the average of 20 loocv, including situations in which the static formulation both correctly and incorrectly classified the task. In fact, task recognition rates for the static formulation across observation ratios is shown in Table II. Evidently,

TABLE II
TASK RECOGNITION RATE FOR STATIC OBSERVATION RATIOS IN EXP. 2.

	Down	Left	Right	Up
0.1	0.53	0.58	0.47	0.89
0.3	0.53	0.68	0.42	0.95
0.5	0.68	0.74	0.32	0.95
0.7	0.74	0.89	0.63	0.95
0.9	0.89	1.00	1.00	1.00

in many cases the task recognition rate, especially when the observation ratio is around half the trajectory or less, recognition rates are equal to chance or worse. As more observations come in, rates increase. The exception is the “Up” trajectory which had better recognition.

There are major trends across all error measures. The dynamic formulation always outperformed the static formulation. Dynamic observations with the longest duration

Comparative performance evaluation for averaged results between the three handover tasks in Exp. 1 and the four diverging tasks in Exp. 2

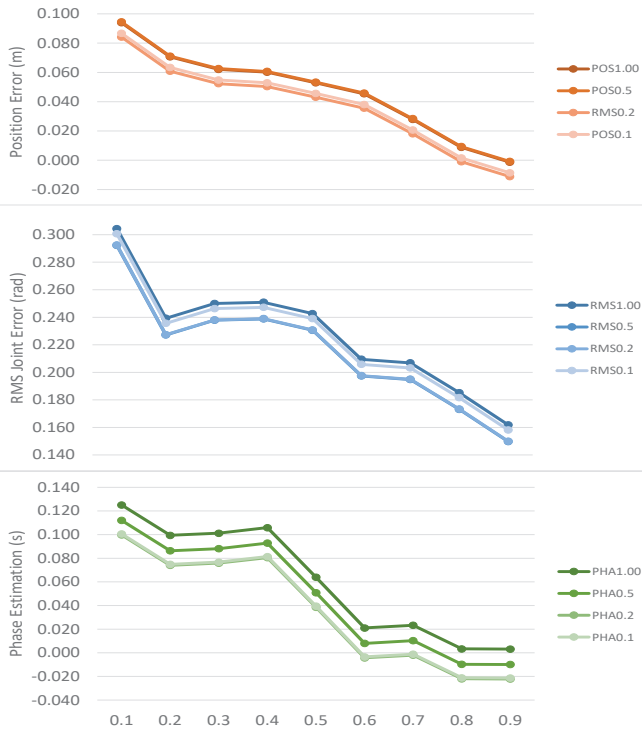


Fig. 6. Comparative performance evaluation for averaged results between the three handover tasks in Exp. 1 and the four diverging tasks in Exp. 2. Averaged results in the static case occurs across observation ratio and for the dynamic case across dynamic observation window duration. The figure’s three plots consist of: (top) final Cartesian position error difference, (middle) difference in RMS joint trajectory error at each time step, and (bottom) final position phase estimation error difference. Positive results indicate a better performance by the dynamic formulation.

did better but nonetheless the performance of the other windows was almost very similar, making it possible to gain responsiveness for a small loss in accuracy. Finally, and most importantly is the fact that the static distribution begin with large errors in the first half of the observations and then register quick drops when more than half of the trajectory has been observed.

As for Cartesian goal position error difference at the end of the task, the static formulation begins with errors differences of 0.1m. The average performance of the dynamic formulation was 0.04m: a difference that is more than double. Hence, particularly at the beginning, the static formulation struggles to correctly classify the true trajectory and generates motion that have more than double the inaccuracy the the average of the dynamic formulation. As for the RMS joint angle error, the same story occurs here. An error difference larger than 0.3rad occurred, almost double the average value for the dynamic formulation which yielded 0.14rad. As for the phase estimation error, the error difference was 0.13s. The average performance of the dynamic formulation was 0.17s.

V. DISCUSSION AND CONCLUSION

This work showed that when the IProMP framework with Phase Estimation is deployed with dynamic human observation windows, the accuracy and responsiveness of the predictive generated robot motions increase significantly. The result occurred across a wide variety of motions and objects, including instances where trajectories begin with similar motions and end with diverging ones—not unlike natural human movements. The approach still suffers from appropriate robot motion generation if the observation was not included in training. We are considering the idea of projecting existing probabilistic distributions to newly observed spaces if we are confident the task type is similar. Also, sometimes the predicted motion reaches the limits of a robot’s arm workspace. In this case, we are considering querying the other robot arm to successfully complete the task.

VI. ACKNOWLEDGEMENTS

This work is supported by “Major Project of the Guangdong Province Department for Science and Technology (2014B090919002), (2016B0911006).”

REFERENCES

- [1] G. Maeda, M. Ewerton, R. Lioutikov, H. B. Amor, J. Peters, and G. Neumann, “Learning interaction for collaborative tasks with probabilistic movement primitives,” in *Humanoid Robots (Humanoids), 2014 14th IEEE-RAS International Conference on*. IEEE, 2014, pp. 527–534.
- [2] G. Maeda, M. Ewerton, G. Neumann, R. Lioutikov, and J. Peters, “Phase estimation for fast action recognition and trajectory generation in human–robot collaboration,” *The International Journal of Robotics Research*, p. 0278364917693927, 2017.
- [3] M. Ewerton, G. Neumann, R. Lioutikov, H. B. Amor, J. Peters, and G. Maeda, “Learning multiple collaborative tasks with a mixture of interaction primitives,” in *Robotics and Automation (ICRA), 2015 IEEE International Conference on*. IEEE, 2015, pp. 1535–1542.
- [4] D. Vogt, S. Stepputtis, S. Grehl, B. Jung, and H. B. Amor, “A system for learning continuous human-robot interactions from human-human demonstrations,” in *Robotics and Automation (ICRA), 2017 IEEE International Conference on*. IEEE, 2017, pp. 2882–2889.
- [5] J. S. Park, C. Park, and D. Manocha, “I-planner: Intention-aware motion planning using learning based human motion prediction,” *arXiv:1608.04837v5*, 2017.
- [6] R. Luo, R. Hayne, and D. Berenson, “Unsupervised early prediction of human reaching for human–robot collaboration in shared workspaces,” *Autonomous Robots*, pp. 1–18, 2017.
- [7] J. Mainprice and D. Berenson, “Human-robot collaborative manipulation planning using early prediction of human motion,” in *Intelligent Robots and Systems (IROS), 2013 IEEE/RSJ International Conference on*. IEEE, 2013, pp. 299–306.
- [8] G. Maeda, A. Maloo, M. Ewerton, R. Lioutikov, and J. Peters, “Anticipatory interaction primitives for human-robot collaboration,” in *2016 AAAI Fall Symposium Series*, 2016.
- [9] A. Paraschos, C. Daniel, J. R. Peters, and G. Neumann, “Probabilistic movement primitives,” in *Advances in neural information processing systems*, 2013, pp. 2616–2624.
- [10] S. Manschitz, M. Gienger, J. Kober, and J. Peters, “Mixture of attractors: A novel movement primitive representation for learning motor skills from demonstrations,” *IEEE Robotics and Automation Letters*, vol. 3, no. 2, pp. 926–933, 2018.
- [11] L. Chen, H. Wu, S. Duan, Y. Guan, and J. Rojas, “Learning human-robot collaboration insights through the integration of muscle activity in interaction motion models,” in *Humanoid Robotics (Humanoids), 2017 IEEE-RAS 17th International Conference on*. IEEE, 2017, pp. 491–496.